

Nanoscale

Accepted Manuscript



This is an *Accepted Manuscript*, which has been through the Royal Society of Chemistry peer review process and has been accepted for publication.

Accepted Manuscripts are published online shortly after acceptance, before technical editing, formatting and proof reading. Using this free service, authors can make their results available to the community, in citable form, before we publish the edited article. We will replace this *Accepted Manuscript* with the edited and formatted *Advance Article* as soon as it is available.

You can find more information about *Accepted Manuscripts* in the [Information for Authors](#).

Please note that technical editing may introduce minor changes to the text and/or graphics, which may alter content. The journal's standard [Terms & Conditions](#) and the [Ethical guidelines](#) still apply. In no event shall the Royal Society of Chemistry be held responsible for any errors or omissions in this *Accepted Manuscript* or any consequences arising from the use of any information it contains.

Revealing Silent Vibration Modes of Nanomaterials by Detecting Anti-Stokes Hyper-Raman Scattering with Femtosecond Laser Pulses

Cite this: DOI: 10.1039/x0xx00000x

Received 00th August 2015,
Accepted 00th August 2015

DOI: 10.1039/x0xx00000x

www.rsc.org/

Jianhua Zeng,^a Lei Chen,^a Qiaofeng Dai,^a Sheng Lan*^a and Shaolong Tie*^b

We proposed a scheme in which normal Raman scattering is coupled with hyper-Raman scattering for generating strong anti-Stokes hyper-Raman scattering in nanomaterials by using femtosecond laser pulses. The proposal was experimentally demonstrated by using single-layer MoS₂ on a SiO₂/Si substrate, 17 nm-thick MoS₂ on an Au/SiO₂ substrate and 9 nm-thick MoS₂ on a SiO₂-SnO₂/Ag/SiO₂ substrate which were confirmed to be highly efficient for second harmonic generation. Strong anti-Stokes hyper-Raman scattering was also observed in other nanomaterials possessing large second-order susceptibilities, such as silicon quantum dots self-assembled into “coffee” rings and tubular Cu-doped ZnO nanorods. In all cases, many Raman inactive vibration modes were clearly revealed in the anti-Stokes hyper-Raman scattering. Apart from strong anti-Stokes hyper-Raman scattering, Stokes hyper-Raman scattering with small Raman shifts was detected during the ablation process of thick MoS₂ layers. It was also observed by slightly defocusing the excitation light. The detection of anti-Stokes hyper-Raman scattering may serve as a new technique for studying the Raman inactive vibration modes in nanomaterials.

1 Introduction

Raman scattering in which the scattered photons carry the information of the target material has been developed as a powerful technique for material analysis. Although both Stokes and anti-Stokes components are expected to appear in a Raman scattering spectrum, only the Stokes component is observed in most cases because of the much larger population of the ground state. In the cases when the excitation intensity of the laser light is sufficiently strong, one can anticipate the observation of second-order Raman (or hyper-Raman) scattering whose intensity is much weaker than the first-order one. Hyper-Raman scattering was demonstrated many years ago by using high-power nanosecond or picosecond lasers.¹⁻⁵ Since some vibration modes are Raman inactive but hyper-Raman active due to the different symmetry selection rules,⁶⁻¹⁰ hyper-Raman scattering has become a complementary tool of normal Raman scattering for revealing silent vibration modes that are invisible in both Raman and infrared absorption spectra.

So far, most hyper-Raman scattering measurements are performed by using nanosecond or picosecond lasers with large average powers and low repetition rates.^{1-5, 11-16} In this case, the

Stokes hyper-Raman component is found to be much stronger than the anti-Stokes one, similar to that observed in normal Raman scattering. The advantage of using nanosecond and picosecond lasers is the narrow linewidth of the laser pulses which offers a good spectral resolution for the vibration modes. However, the long pulse width and low repetition rate of nanosecond and picosecond lasers generally lead to a long integration time (e.g., several hours or one day) for the weak hyper-Raman scattering signal.^{2,4} For this reason, femtosecond (fs) lasers with large peak powers and high repetition rates have been employed in the excitation of hyper-Raman scattering signal.¹⁷⁻¹⁹ It was found that hyper-Raman scattering signal could be efficiently generated and the integration time was significantly reduced to a few seconds.^{18,19} More interestingly, it was noticed that the intensity of the anti-Stokes hyper-Raman component was comparable or even stronger than that of the Stokes one.¹⁸ This behavior is quite important because in some cases the observation of Stokes hyper-Raman scattering is severely disturbed by other nonlinear optical signals such as two-photon-induced luminescence when fs lasers are used. Previously, the second harmonic generation (SHG) of silicon

(Si) nanoparticles was investigated by using fs laser pulses and strong anti-Stokes hyper-Raman scattering was observed together with the extremely efficient SHG.²⁰ The phenomena described above indicate the possibility of generating highly efficient anti-Stokes hyper-Raman scattering by using fs laser pulses with high repetition rates and also raise the question why anti-Stokes hyper-Raman scattering appears to be much stronger than Stokes one in the case of fs laser excitation.

If we review the physical mechanism for the well-established technique of coherent anti-Stokes Raman scattering,²¹ which is shown in Fig. 1(a), we can easily propose a scheme for generating highly efficient anti-Stokes hyper-Raman scattering by utilizing the coupling between normal

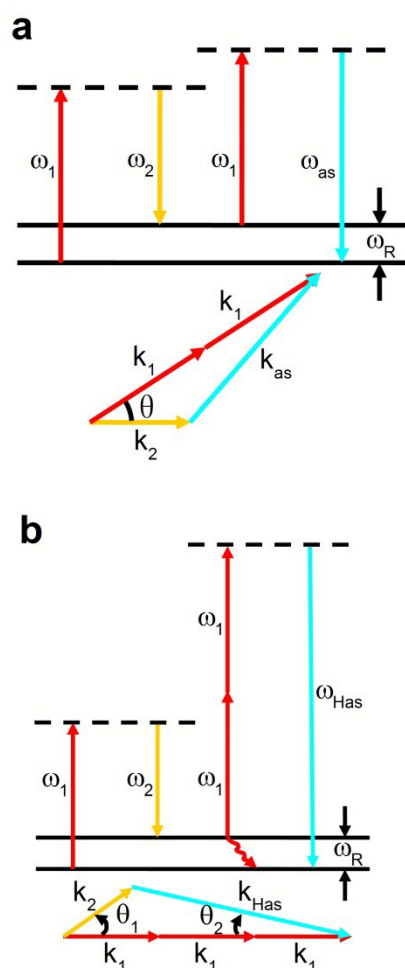


Fig. 1 (a) Principle of the coherent anti-Stokes Raman scattering technique. The emission of an anti-Stokes Raman scattering photon (ω_{as}) is induced by the interaction of two photons (ω_1 and ω_2) with a frequency difference equal to ω_R . The relationship between the wavevectors of the four photons involved in the coherent anti-Stokes scattering process is shown in the inset. (b) Schematic showing the coupling between a normal Raman scattering and a hyper-Raman scattering. The population of the excited state is induced by the normal Raman scattering ($\omega_1 \rightarrow \omega_2$). The transition from the excited state to the virtual state and the emission of an anti-Stokes hyper-Raman scattering photon is induced by the hyper-Raman scattering process ($2\omega_1 \rightarrow \omega_{Has}$). The relationship between the wavevectors of the five photons involved in the coupled scattering process is shown in the inset.

Raman and hyper-Raman scattering processes, as shown in Fig. 1(b). In this case, the effective population of the excited state is induced by the Raman scattering process. After that, the transition to a virtual state can be achieved by simultaneously absorbing two photons of the fundamental light provided that the transition rate is larger than the decay rate of the excited state to the ground state. Apparently, such a condition can be satisfied by using fs laser pulses with large peak powers and high repetition rates and nanomaterials with large second-order nonlinear susceptibilities ($\chi^{(2)}$) which render a large transition rate from the excited state to the virtual state.

In general, nanometer-sized materials possess much larger second-order nonlinear susceptibilities ($\chi^{(2)}$) as compared with their bulk counterparts. For bulk materials with centrosymmetry such as Si and gold (Au), their second-order nonlinear susceptibilities ($\chi^{(2)}$) are expected to vanish. However, it has been shown that Si and Au nanoparticles exhibit efficient SHG because of the deviation from symmetric shape and the breaking of symmetry at interfaces.^{20,22,23} For two-dimensional materials such as MoS₂, efficient SHG was observed only in MoS₂ with odd layers especially single-layer MoS₂.²⁴⁻²⁹ The $\chi^{(2)}$ of single-layer MoS₂ ($\sim 10^{-7}$ m/V) was found to be seven orders of magnitude larger than that of bulk MoS₂ ($\sim 10^{-14}$ m/V).²⁴ Similar behavior was observed in ZnO and other semiconductors. For bulk ZnO, the $\chi^{(2)}$ was found to be $\sim 10^{-11}$ m/V while that of ZnO quantum dots (QDs) was determined to be $\sim 10^{-9}$ m/V.³⁰ Besides, a large $\chi^{(2)}$ of $\sim 10^{-4}$ m/V was found in InAs/GaAs self-assembled QDs.³¹ All these phenomena clearly indicate that the proposed scheme is highly suitable for detecting the silent vibration modes in nanomaterials.

In this article, we demonstrated the proposal mainly by using MoS₂, a two-dimensional material which has attracted tremendous interest in recent years because of its potential applications in the fabrication of electronic and photonic devices.³²⁻⁴¹ In addition, we also confirmed, by using Si QDs self-assembled into “coffee” rings and tubular Cu-doped ZnO nanorods (NRs) as examples, that the observation of strong anti-Stokes hyper-Raman scattering is a popular phenomenon when nanomaterials with large $\chi^{(2)}$ are excited by fs laser pulses. The detection of anti-Stokes hyper-Raman scattering may become a new technique for studying the Raman inactive vibration modes in nanomaterials.

2 Experimental section

Several nanomaterials were chosen to study the proposed anti-Stokes hyper-Raman scattering by using fs laser excitation, including thin MoS₂ layers on different substrates, Si QDs self-assembled into “coffee” rings, and tubular Cu-doped ZnO NRs. The common feature of these nanomaterials is the verified large $\chi^{(2)}$ and efficient SHG.

In our experiments, Si QDs were prepared *via* a chemical etching by using Si powder as precursor and the mixture of 60 wt% HNO₃ and 46 wt% HF as solution, respectively. The detailed description can be found in previous literature.⁴² The transmission electron microscopy observation revealed that the

diameter of the obtained Si ODs was 2 ± 0.25 nm. It was found that Si QDs were self-assembled into “coffee” rings after the evaporation of water. Such “coffee” rings composed of Si QDs exhibited strong SHG under the excitation of fs laser pulses. The detailed method for preparing tubular Cu-doped ZnO NRs can be found in our recent publication.⁴³ MoS₂ layers were exfoliated on a SiO₂/Si substrate with a 300 nm-thick SiO₂ film, an Au/SiO₂ substrate composed of a 50 nm-thick Au film on a silica substrate of ~ 360 μm , and a SiO₂-SnO₂/Ag/SiO₂ substrate composed of a 20 nm-thick SiO₂-SnO₂ layer and a 50 nm-thick Ag film on a silica substrate of ~ 360 μm (see ESI, Fig. S1(a)). The colors exhibited by the MoS₂ layers on different substrates were examined under a microscope. Basically, we can easily calculate the reflection spectrum of a thin MoS₂ layer with a certain thickness and deduce the chromaticity coordinate of the MoS₂ layer. By correlating the calculated chromaticity coordinate with the actually observed color, one can give a rough estimation for the thickness of the MoS₂ layer (see ESI, Fig. S2). The normal Raman spectra of the MoS₂ layers were measured by using a Raman spectrometer (Invia, Renishaw) at excitation wavelengths of 514 and 785 nm (see ESI, Fig. S3).

The fs laser light with a repetition rate of 76 MHz and a duration of 130 fs delivered by a fs oscillator (Mira 900S, Coherent) was focused on the nanomaterials by using the 60 \times objective lens (NA = 0.85) of an inverted microscope (Axio Observer A1, Zeiss). The nonlinear optical signals generated by the nanomaterials were collected by using the same objective lens and directed to a combination of a spectrometer (SR-500i-B1, Andor) and a coupled-charge device (DU970N, Andor) for analysis (see ESI, Fig. S1(b)).

3 Results and discussion

3.1 Anti-Stokes hyper-Raman scattering observed in single-layer MoS₂ on a SiO₂/Si substrate

Since single-layer MoS₂ on a SiO₂/Si substrate was known to possess a large $\chi^{(2)}$,²⁴⁻²⁹ we first examined the linear and nonlinear optical responses of a single-layer MoS₂ whose microscope image is shown in the inset of Fig. 2(a). The Raman spectra of the single-layer MoS₂ were measured at two different excitation wavelengths of 514 and 785 nm, as shown in Fig. 2(a). The Raman signal obtained at 514 nm, which is presented in the inset, was much stronger than that obtained at 785 nm because of the resonant excitation of the single-layer MoS₂ with a bandgap energy of ~ 1.9 eV.^{44,45} Two peaks located at 384.5 cm⁻¹ and 403.1 cm⁻¹, which are attributed to the in-plane (E_{2g}^1) and out-of-plane (A_{1g}) vibration modes, were clearly resolved. The MoS₂ layer was confirmed to be a single-layer one by the frequency difference between the two modes which is estimated to be 18.6 cm⁻¹.⁴⁶ No anti-Stokes Raman scattering was observed in the Raman spectra.

In Figs. 2(b), we present the nonlinear response spectra of the single-layer MoS₂ measured by using a fs laser light at 750 nm. The exposure time of the CCD, which corresponds to the integration time of the nonlinear optical signals, was chosen to

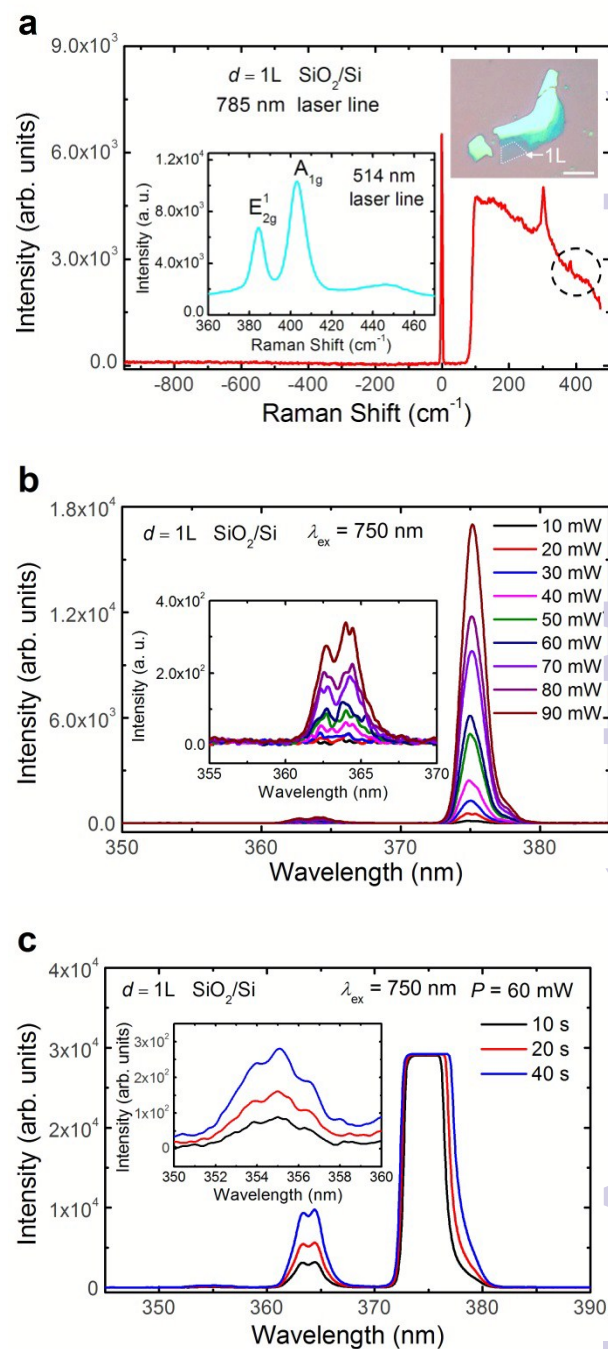


Fig. 2 (a) Raman scattering spectrum measured at 785 nm. The in-plane (E_{2g}^1) and out-of-plane (A_{1g}) vibration modes are indicated by the dashed circle. The Raman spectrum measured at 514 nm in which the two vibration modes are clearly resolved and the microscope image of the single-layer MoS₂ on the SiO₂/Si substrate are shown in the inset. The length of the scale bar is 10 μm . (b) Nonlinear response spectra of the single-layer MoS₂ measured at different excitation powers with an exposure time of 0.5 s. The anti-Stokes hyper-Raman signal is magnified in the inset. (c) Nonlinear response spectra of the single-layer MoS₂ measured at an excitation power of 60 mW with different exposure times of 10, 20, and 40 s. In this case, the intensity of the SHG was beyond the detection region of the CCD. The weak anti-Stokes hyper-Raman signal with a larger Raman shift appearing in the 350-360 nm wavelength range is magnified in the inset.

be 0.5 s. Apart from the strong second harmonic (SH) observed at 375 nm, one can see a nonlinear signal composed of two peaks appearing at the short-wavelength side of the SH (see the inset of Fig. 2(b)). They are attributed to the anti-Stokes hyper-Raman scattering related to two vibration modes with Raman shifts of about 793 cm^{-1} and 923 cm^{-1} , respectively. These two modes are not found in the normal Raman spectrum of MoS_2 .⁴⁷ Contrary to the normal Raman scattering, Stokes hyper-Raman scattering was not observed in the nonlinear response spectra of the single-layer MoS_2 . Early in 2000, Nayfeh et al. also observed strong anti-Stokes hyper-Raman scattering in the microcrystalline films composed of ultrasmall Si nanoparticles which exhibited extremely strong SHG.²⁰ In their case, the intensity of the anti-Stokes hyper-Raman scattering was even stronger than that of the SH.

In order to resolve more vibration modes in the nonlinear response spectra, we increased the integration time from 10 to 40 s, as shown in Fig. 2(c). Six vibration modes were clearly revealed and their Raman shifts were estimated to be 772 cm^{-1} , 888 cm^{-1} , 1378 cm^{-1} , 1492 cm^{-1} , 1594 cm^{-1} and 1667 cm^{-1} , respectively (see ESI, Fig. S4 for the details of extracting the Raman shifts of these vibration modes).

In Fig. 1(b), it can be seen that the transition rate from the excited state to the virtual state should be larger than the decay rate of the excited state to the ground state in order to observe the anti-Stokes hyper Raman scattering. In this case, the hyper-Rayleigh scattering, which corresponds to SHG, is also strong because of the large transition rate from the excited state to the virtual state. For this reason, an enhancement in hyper-Raman scattering is also accompanied by an enhancement in SHG, as shown in Fig. 2(c) where the integration time for the nonlinear signals is increased. In other words, any method which can be employed to enhance SHG will also benefit to the enhancement in hyper-Raman scattering.

3.2 Anti-Stokes hyper-Raman scattering observed in 17 nm MoS_2 layer on an Au/SiO_2 substrate

Very recently, we have demonstrated that the SHG of a MoS_2 layer can be enhanced by using a thin gold film.⁴⁸ For the MoS_2 layers on an Au/SiO_2 substrate, the strongest SHG is no longer achieved in single-layer MoS_2 which exhibits the strongest SHG on a SiO_2/Si substrate. Based on the calculation of the enhancement factor for SHG, it was found that the strongest SHG was obtained in the 17 nm-thick MoS_2 layer on the Au/SiO_2 substrate.⁴⁸ Therefore, we measured the nonlinear response spectra for the 17 nm-thick MoS_2 layer on the Au/SiO_2 substrate, as shown in Fig. 3. In Fig. 3(a), we present the evolution of the nonlinear response spectrum obtained at 800 nm with increasing excitation power. The dependence of the SHG intensity on the excitation power is provided in the inset where a slope of ~ 2.28 was extracted by fitting the experimental data plotted in a double logarithmic coordinate, in good agreement with the second-order nature of SHG. In Fig. 3(b), strong anti-Stokes hyper-Raman scattering was observed at an excitation power of 80 mW. In this case, the intensity of the SHG exceeded the detection range of the CCD. In order to see clearly the hyper-Raman scattering, the spectra were magnified in the wavelength range of 382–394 nm, as shown in the inset. The intensity of the hyper-Raman scattering was

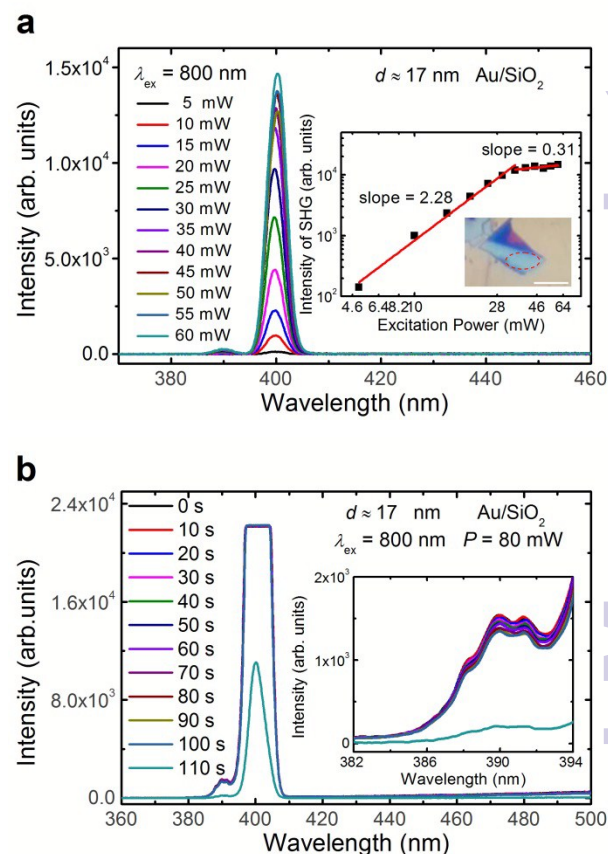


Fig. 3 (a) Evolution of the nonlinear response spectrum with increasing excitation intensity measured at 800 nm with 50 gain value for the 17 nm-thick MoS_2 layer on the Au/SiO_2 substrate. The integration time was chosen to be 0.5 s. The dependence of the SHG intensity on the excitation intensity and the microscope image of the 17 nm-thick MoS_2 layer on the Au/SiO_2 substrate included within the dotted ellipse is shown in the inset. The length of the scale bar is 10 μm . (b) Evolution of the nonlinear response spectrum with increasing irradiation time measured at an excitation intensity of 80 mW for the 17 nm-thick MoS_2 layer on the Au/SiO_2 substrate. The integration time was chosen to be 10 s. In this case, the intensity of the SHG was beyond the detection region of the CCD.

found to increase with increasing integration time. However, it does not exhibit a linear increase because of the saturation of the SHG for excitation powers larger than 35 mW (see the inset of Fig. 3(a)). When the ablation of the MoS_2 layer occurred, decrease in both the SHG and the hyper-Raman scattering was observed, as shown in Fig. 3(b). The Raman shifts for the four vibration modes resolved in the anti-Stokes hyper-Raman scattering were derived to be $\sim 542\text{ cm}^{-1}$, $\sim 655\text{ cm}^{-1}$, $\sim 761\text{ cm}^{-1}$ and $\sim 846\text{ cm}^{-1}$ (see ESI, Fig. S4 and Table S1/S2 for the details of extracting the Raman shifts of these vibration modes). These four vibration modes are also not found in the normal Raman spectrum of MoS_2 .⁴⁷ In addition, it is noticed that the vibration modes observed in the 17 nm-thick MoS_2 layer on the Au/SiO_2 substrate are different from those observed in the single-layer MoS_2 on the SiO_2/Si substrate. Apart from the difference in thickness, this behavior implies that the enhancement in hyper-Raman scattering provided by the thin gold film is selective. More experiments are needed to clarify this issue.

3.3 Stokes hyper-Raman scattering observed in the ablation of MoS_2 layers

When the excitation power of the fs laser light exceeds a critical value, the ablation of the MoS₂ layer will occur, leading to the reduction in the thickness. Since the maximum SHG is achieved in the 17 nm-thick MoS₂, a decrease in SHG is expected with the decrease of the thickness. In the inset of Fig. 4(a), we present the microscope images of the 17 nm-thick MoS₂ layer before and after the ablation. A color change was

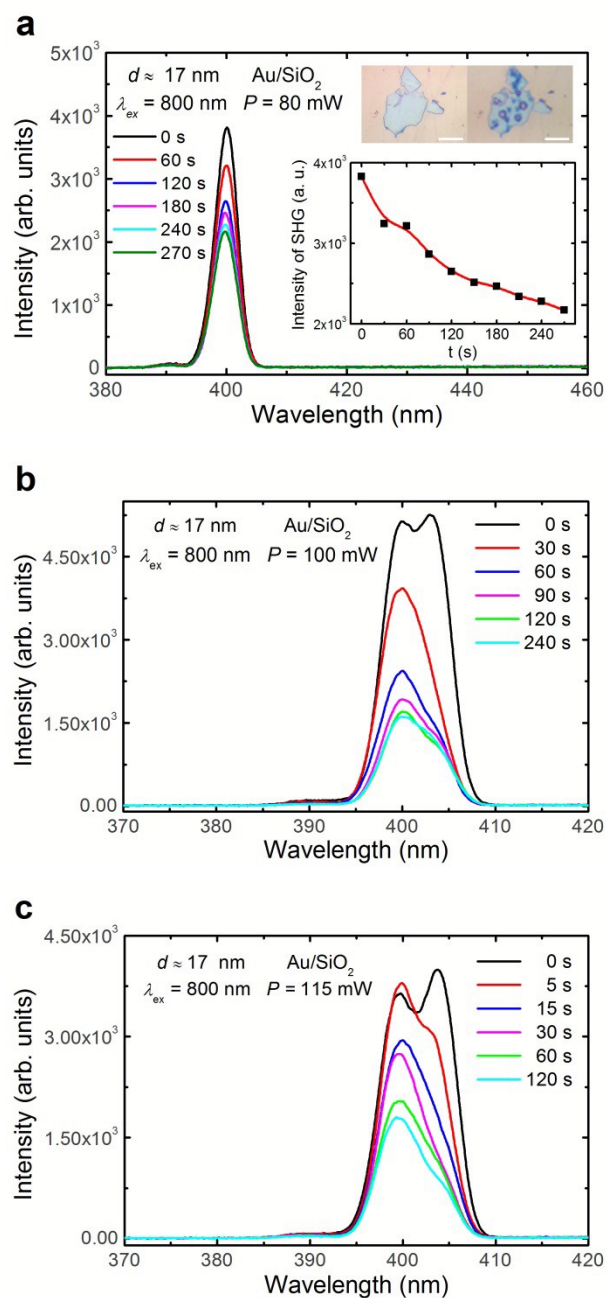


Fig. 4 (a) Evolution of the nonlinear response spectrum of the 17 nm-thick MoS₂ on the Au/SiO₂ substrate with increasing ablation time observed at an excitation power of 80 mW. The dependence of the SHG intensity on the ablation time and microscope images of the 17 nm-thick MoS₂ before and after the ablation by using high-power fs laser light are shown in the inset. The length of the scale bar is 10 μ m. (b) and (c): Evolution of the nonlinear response spectrum with increasing ablation time observed at excitation powers of 100 and 115 mW, respectively. In all cases, the integration time was all chosen to be 0.5 s.

observed at the ablation points. In Fig. 4(a), we show the evolution of the nonlinear response spectrum with increasing ablation time when the excitation power was fixed at 80 mW. In this case, a monotonic reduction in the SHG intensity was observed with increasing ablation time, as summarized in the inset. If we raised the excitation power further to 100 or 115 mW, a new peak whose intensity is comparable to that of the SH emerged at the long-wavelength side of the SH, as can be seen in Figs. 4(b) and 4(c). We attributed this peak to the Stokes hyper-Raman scattering of a certain vibration mode whose Raman shift was estimated to be about 270 cm⁻¹ (see ESI, Fig. S4 and Table S1/S2). With increasing ablation time, the intensity of the Stokes hyper-Raman scattering decreased and finally appeared as a shoulder on the right side of the SH.

When the MoS₂ layer was ablated by the high-power fs laser light, the high temperature in MoS₂ accelerated the decay of electrons from the excited state to the ground state. As a result, the excited state is no longer effectively populated, leading to the decoupling between the normal Raman scattering and the hyper-Raman scattering proposed in Fig. 1(b). In this case, the anti-Stokes hyper-Raman scattering was reduced while the Stokes component became visible in the nonlinear response spectra because of the increased population of the ground state, as evidenced in Fig. 3(b) and Fig. 4.

Basically, MoS₂ possesses semiconducting 2H phase and metallic 1T/1T' phase.⁴⁹⁻⁵² While the 2H phase is thermodynamically stable, the 1T phase is inherently unstable or metastable. The conversion of 2H phase to 1T phase can be realized through the intercalation of alkali-metal (Li and K) due to the charge transfer from alkali atoms to MoS₂.⁴⁹⁻⁵² Very recently, it has been demonstrated experimentally that the reversion of the 1T phase to the 2H phase can be realized by irradiating fs laser pulses, making it possible to fabricate a 1T/1T' to 2H heterojunction.⁴⁹ It is noticed, however, that the fs laser power used to induce the phase transition was only 150 μ W and an ablation of MoS₂ occurred when a higher laser power was employed. Physically, the possibility of introducing a phase transition from 2H to 1T/1T' by using fs laser irradiation is quite small because the former is stable while the latter is metastable. As compared with metallic 1T/1T'–MoS₂, the absorption of laser energy by semiconducting 2H–MoS₂ is much smaller. Consequently, the fs laser power we used was almost three orders of magnitude larger than that reported for inducing the 1T/1T' to 2H phase transition. In order to confirm that the change in SHG intensity and film color was caused by ablation rather than phase transition, we measured the Raman scattering spectra for the un-ablated and ablated areas and found no change in the Raman scattering peaks (see ESI, Fig. S3b). This result indicates that the irradiation of fs laser pulses results in the ablation of MoS₂ rather than the 2H to 1T/1T' phase transition.

3.4 Stokes hyper-Raman scattering observed in the case of defocusing

Previously, it was shown that the third harmonic generation (THG) and the associated hyper-Raman scattering exhibited a conical emission due to the phase-matched condition (eq. (1)).

momentum conservation) that needs to be satisfied in the nonlinear optical process.¹⁸ Since the wavevector of the anti-Stokes hyper-Raman scattering is larger than that of the Stokes one, the conical angle for the anti-Stokes component should be smaller while that for the Stokes one should be larger than that of the THG. Similar situation is expected in the hyper-Raman scattering associated with SHG as we studied in this work. For

SnO₂/Ag/SiO₂ substrate by using focused fs laser light and the increased integration time from 0.5 to 20 s.

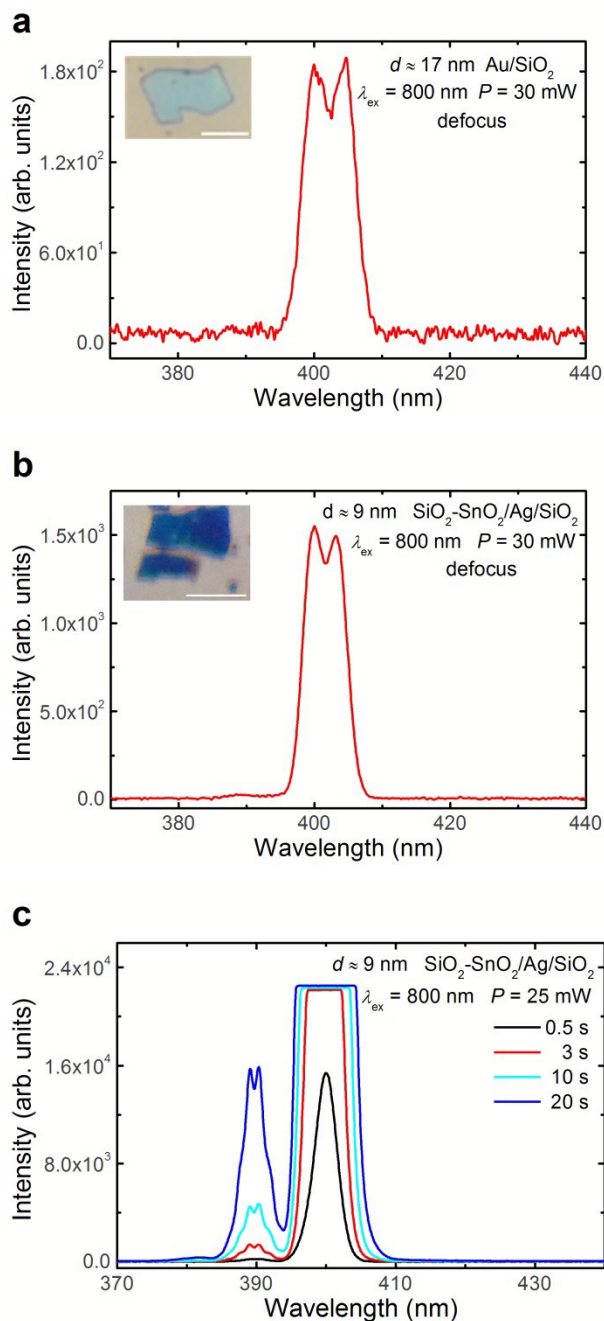


Fig. 5 Nonlinear response spectra measured by using defocused fs laser light for the 17 nm-thick MoS₂ layer on the Au/SiO₂ substrate (a) and the 9 nm-thick MoS₂ layer on the SiO₂-SnO₂/Ag/SiO₂ substrate (b). The microscope images for the corresponding MoS₂ layers are shown in the insets. The length of the scale bar is 10 μm. (c) Nonlinear response spectra measured for the 9 nm-thick MoS₂ layer on the SiO₂-

this reason, the Stokes hyper-Raman component may not be collected by the objective in the case of focusing because of the larger conical angle, especially for those vibration modes with large Raman shifts. A possible way to observe the Stokes hyper-Raman scattering with small Raman shifts is to increase the conical angle for collecting signals by moving the objective towards the sample or by defocusing upwards. In this way, the signals with conical angles larger than the incident angle can be collected by the objective, enabling the observation of the Stokes hyper-Raman scattering with small Raman shifts. However, the excitation intensity is also reduced by defocusing, leading to the reduction in the intensity of the SHG and hyper-Raman scattering. In Fig. 5(a), we show the nonlinear response spectra measured for a 17 nm-thick MoS₂ layer on the Au/SiO₂ substrate by using defocused fs laser light at 800 nm. In this case, the anti-Stokes hyper-Raman scattering was too weak to be observed. As expected, the Stokes component with a Raman shift of 278 cm⁻¹ was clearly resolved in the spectrum, similar to the Stokes component observed in the ablation process of the MoS₂ layer. If we refocused the excitation light on the MoS₂ layer, the Stokes component disappeared and the anti-Stokes component appeared. We also examined the nonlinear response spectrum for a 9 nm-thick MoS₂ layer on a SiO₂-SnO₂/Ag/SiO₂ substrate which exhibited very strong SHG even in the case of defocusing, as shown in Fig. 5(b). A Stokes hyper-Raman scattering with a Raman shift of 226 cm⁻¹ was observed. Actually, the observation of Stokes hyper-Raman scattering with less strong laser field similar to the case of defocusing was also found in the study of the hyper-Raman scattering spectrum of hydrogen atoms.⁵³ Similarly, strong anti-Stokes hyper-Raman scattering was revealed in the nonlinear response spectra of the 9 nm-thick MoS₂ layer on the SiO₂-SnO₂/Ag/SiO₂ substrate by increasing the integration time from 0.5 to 20 s, as shown in Fig. 5(c). Their Raman shifts were calculated to be 527 cm⁻¹, 620 cm⁻¹, 703 cm⁻¹, and 792 cm⁻¹ respectively (see ESI, Fig. S4 and Table S1/S2).

3.5 Anti-Stokes hyper-Raman scattering observed in Si QDs and ZnO NRs

As depicted in Fig. 1(b), the transition rate from the excited state to the virtual state is determined not only by the excitation intensity but also by the $\chi^{(2)}$ of the nanomaterials which is indirectly reflected in the efficiency of the hyper-Rayleigh scattering or the intensity of SHG. Therefore, anti-Stokes hyper-Raman scattering should also be observed in other nanomaterials with large $\chi^{(2)}$. Here, we show two typical examples where strong anti-Stokes hyper-Raman scattering was successfully observed. The first one is Si QDs self-assembled into “coffee” rings. Such a nanomaterial is quite similar to the microcrystallite films composed of ultrasmall Si nanoparticles reported previously.²⁰ The second one is tubular Cu-doped ZnO NRs. The nonlinear response spectra measured for these two nanomaterials are presented in Figs. 6(a) and 6(b) while the scanning electron microscope (SEM) images are shown in the insets. The magnified spectra showing clearly the anti-Stokes hyper-Raman scattering are also provided as insets. For the Si QDs, four vibration modes with Raman shift of about 578 cm⁻¹, 666 cm⁻¹, 763 cm⁻¹, 859 cm⁻¹ are deduced (see ESI, Fig. S4). They are not found in the Raman scattering spectrum of Si.^{54,55} Similarly, two peaks with Raman shifts of about 859 cm⁻¹ and 995 cm⁻¹ were clearly identified in the anti-Stokes hyper-

Raman scattering of the tubular Cu-doped ZnO NRs (see ESI, Fig. S4 and Table S1/S2). These two vibration modes are also not found in the Raman scattering spectrum of ZnO.⁵⁶⁻⁵⁹

The authors acknowledge the financial support from the National Natural Science Foundation of China (Grant Nos. 51171066 and 11374109).

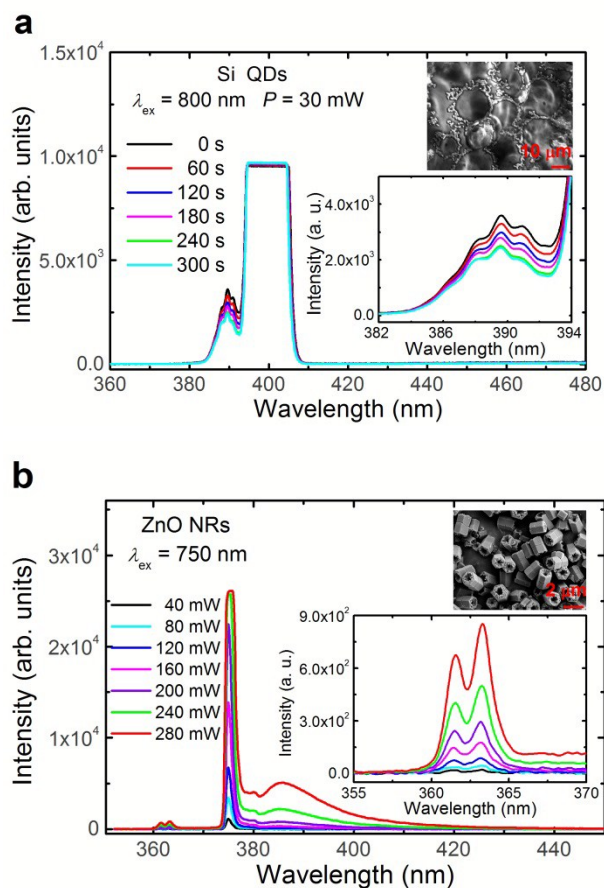


Fig. 6 (a) Evolution of the nonlinear response spectrum with increasing integration time measured for the Si QDs self-assembled into coffee rings. The excitation wavelength was chosen to be 800 nm and the excitation power was fixed at 30 mW. The SEM image of the self-assembled Si QDs and the magnified anti-Stokes hyper-Raman scattering are shown in the insets. (b) Evolution of the nonlinear response spectrum with increasing excitation power measured for the tubular Cu-doped ZnO NRs. The excitation wavelength and the integration time were chosen to be 750 nm and 0.5 s, respectively. The SEM image of the tubular Cu-doped ZnO NRs and the magnified anti-Stokes hyper-Raman scattering are shown in the insets.

4 Conclusion

In summary, we proposed a scheme for generating anti-Stokes hyper-Raman scattering by using fs laser pulses and demonstrated the proposal by using MoS₂ layers on different substrates, Si QDs self-assembled into “coffee” rings and tubular Cu-doped ZnO NRs that exhibited efficient SHG. In addition, Stokes hyper-Raman scattering was observed in the ablation process of MoS₂ layers and also in the case of defocusing the excitation light. With appropriate improvement, the detection of strong anti-Stokes hyper-Raman scattering may become a new technique for studying the Raman inactive vibration modes in nanomaterials.

Acknowledgements

Notes and references

^aGuangdong Provincial Key Laboratory of Nanophotonic Functional Materials and Devices, School of Information and Optoelectronic Science and Engineering, South China Normal University, Guangzhou 510006, P. R. China. E-mail: slan@scnu.edu.cn

^bSchool of Chemistry and Environment, South China Normal University, Guangzhou 510006, P. R. China. E-mail: tiesl@scnu.edu.cn

†Electronic Supplementary Information (ESI) available. See DOI: 10.1039/b000000x/

- H. Vogt, *Phys. Rev. B*, 1988, **38**, 5699-5708.
- K. Inoue and K. Watanabe, *Phys. Rev. B*, 1989, **39**, 1977-1980.
- K. Watanabe and K. Inoue, *J. Phys. Soc. Jpn.*, 1989, **58**, 726-732.
- Y. Tezuka, S. Shin and M. Ishigame, *Phys. Rev. B*, 1994, **49**, 9317-9321.
- K. Watanabe, K. Inoue and F. Minami, *Phys. Rev. B*, 1992, **46**, 2024-2033.
- S. J. Cyvin, J. E. Rauch and J. C. Decius, *J. Chem. Phys.*, 1965, **43**, 4083-4095.
- J. H. Christie and D. J. Lockwood, *J. Chem. Phys.*, 1971, **54**, 1144-1154.
- D. L. Andrews and T. Thirunamachandran, *J. Chem. Phys.*, 1978, **68**, 2941-2951.
- W. P. Acker, D. H. Leach and R. K. Chang, *Chem. Phys. Letters*, 1989, **155**, 491-495.
- A. V. Baranov, Y. S. Bobovich and V. I. Petrov, *Sov. Phys. Usp.*, 1990, **33**, 812-832.
- H. Vogt and G. Neumann, *Phys. Status Solidi B*, 1979, **92**, 57-63.
- H. Vogt, J. A. Sanjurjo and G. Rossbroich, *Phys. Rev. B*, 1982, **26**, 5904-5910.
- A. V. Baranov, K. Inoue, K. Toba, A. Yamanaka, V. I. Petrov and A. V. Fedorov, *Phys. Rev. B*, 1996, **53**, R1721-R1724.
- K. Inoue, A. Yamanaka, K. Toba, A. V. Baranov, A. A. Onushchenko and A. V. Fedorov, *Phys. Rev. B*, 1996, **54**, R8321-R8324.
- M. Mizuno, H. Hamaguchi and T. Tahara, *J. Phys. Chem. A*, 2002, **106**, 3599-3604.
- J. Kneipp, H. Kneipp and K. Kneipp, *PNAS*, 2006, **103**, 17149-17153.
- S. O. Konorov, D. A. Akimov, A. A. Ivanov, M. V. Alfimov and A. M. Zheltikov, *Journal of Experimental and Theoretical Physics*, 2004, **99**, 19-27.
- D. Homoelle, K. D. Moll, A. L. Gaeta and R. W. Boyd, *Phys. Rev. A*, 2005, **72**, 011802(R).
- Fontes, K. Ajito, A. A. R. Neves, W. L. Moreira, A. A. de Thomaz, J. C. Barbosa, A. M. de Paula and C. L. Cesar, *Phys. Rev. E*, 2005, **72**, 012903.
- M. H. Nayfeh, O. Akcakir, G. Belomoin, N. Barry, J. Therrien and J. Gratton, *Appl. Phys. Lett.*, 2000, **77**, 4086-4088.
- A. Zumbusch, G. R. Holtom and X. S. Xie, *Phys. Rev. Lett.*, 1999, **82**, 4142-4145.

- 22 C. Hubert, L. Billot, P. -M. Adam, R. Bachelot, P. Royer, J. Grand, D. Gindre, K. D. Dorkenoo and A. Fort, *Appl. Phys. Lett.*, 2007, **90**, 181105.
- 23 G. Liu, H. Deng, G. Li, L. Chen, Q. Dai, S. Lan and S. Tie, *Plasmonics*, 2014, **9**, 1471–1480.
- 24 N. Kumar, S. Najmaei, Q. Cui, F. Ceballos, P. M. Ajayan, J. Lou and H. Zhao, *Phys. Rev. B*, 2013, **87**, 161403(R).
- 25 L. M. Malard, T. V. Alencar, A. P. M. Barboza, K. F. Mak and A. M. dePaula, *Phys. Rev. B*, 2013, **87**, 201401(R).
- 26 Y. Li, Y. Rao, K. F. Mak, Y. You, S. Wang, C. R. Dean and T. F. Heinz, *Nano Lett.*, 2013, **13**, 3329–3333.
- 27 W. T. Hsu, Z. A. Zhao, L. J. Li, C. H. Chen, M. H. Chiu, P. S. Chang, Y. C. Chou and W. H. Chang, *ACS Nano*, 2014, **8**, 2951–2958.
- 28 X. B. Yin, Z. L. Ye, D. A. Chenet, Y. Ye, K. O'Brien, J. C. Hone and X. Zhang, *Science*, 2014, **344**, 488–490.
- 29 R. Wang, H. C. Chien, J. Kumar, N. Kumar, H. Y. Chiu and H. Zhao, *Appl. Mater. Interfaces*, 2014, **6**, 314–318.
- 30 D. Maikhuri, S. P. Purohit and K. C. Mathur, *AIP Advances*, 2015, **5**, 047115.
- 31 S. Sauvage, T. Brunhes, P. Boucaud, A. Lemaitre, J. -M. Gerard, F. Glotin, R. Prazeres, and J. -M. Ortega, *Phys. Status Solidi B*, 2001, **224**, 595–598.
- 32 L. Liu, S. B. Kumar, Y. Ouyang and J. Guo, *IEEE Trans. Electron Devices*, 2011, **58**, 3042–3047.
- 33 Y. Yoon, K. Ganapathi and S. Salahuddin, *Nano Lett.*, 2011, **11**, 3768–3773.
- 34 H. Wang, L. Yu, Y. -H. Lee, Y. Shi, A. Hsu, M. Chin, L. -J. Li, M. Dubey, J. Kong and T. Palacios, *Nano Lett.*, 2012, **12**, 4674–4680.
- 35 B. Radisavljevic, M. B. Whitwick and A. Kis, *ACS Nano*, 2011, **5**, 9934–9938.
- 36 S. Bertolazzi, J. Brivio and A. Kis, *ACS Nano*, 2011, **5**, 9703–9709.
- 37 Q. He, Z. Zeng, Z. Yin, H. Li, S. Wu, X. Huang and H. Zhang, *Small* 2012, **8**, 2994–2999.
- 38 J. Pu, Y. Yomogida, K. -K. Liu, L. -J. Li, Y. Iwasa and T. Takenobu, *Nano Lett.*, 2012, **12**, 4013–4017.
- 39 Z. Yin, H. Li, H. Li, L. Jiang, Y. Shi, Y. Sun, G. Lu, Q. Zhang, X. Chen and H. Zhang, *ACS Nano*, 2012, **6**, 74–80.
- 40 H. S. Lee, S. -W. Min, Y. -G. Chang, P. M. Kyu, T. Nam, H. Kim, J. H. Kim, S. Ryu and S. Im, *Nano Lett.*, 2012, **12**, 3695–3700.
- 41 M. Shanmugam, T. Bansal, C. A. Durcan and B. Yu, *Appl. Phys. Lett.*, 2012, **100**, 153901.
- 42 K. Sato, H. Tsuji, K. Hirakuri, N. Fukata and Y. Yamauchi, *Chem. Commun.*, 2009, **25**, 3759–3761.
- 43 X. Wan, X. Liang, C. Zhang, X. Li, W. Liang, H. Xu, S. Lan, and S. Tie, *Chem. Eng. J.*, 2015, **272**, 58–68.
- 44 K. F. Mak, C. Lee, J. Hone, J. Shan and T. F. Heinz, *Phys. Rev. Lett.*, 2010, **105**, 136805.
- 45 H. Zeng, J. Dai, W. Yao, D. Xiao and X. Cui, *Nat. Nanotechnol.*, 2012, **7**, 490–493.
- 46 H. Li, Q. Zhang, C. C. R. Yap, B. K. Tay, T. H. T. Edwin, A. Olivier and D. Baillargeat, *Adv. Funct. Mater.*, 2012, **22**, 1385–1390.
- 47 B. C. Windom, W. G. Sawyer and D. W. Hahn, *Tribol Lett.*, 2011, **42**, 301–310.
- 48 J. Zeng, M. Yuan, W. Yuan, Q. Dai, H. Fan, S. Lan and S. Tie, *Nanoscale*, 2015, **7**, 13547–13553.
- 49 Y. Guo, D. Sun, B. Ouyang, A. Raja, J. Song, T. F. Heinz and L. E. Brus, *Nano Lett.*, 2015, **15**, 5081–5088.
- 50 X. Fan, P. Xu, D. Zhou, Y. Sun, Y. C. Li, M. A. T. Nguyen, M. Terrones and T. E. Mallouk, *Nano Lett.*, 2015, **15**, 5956–5960.
- 51 M. Chhowalla, D. Voiry, J. Yang, H. S. Shin and K. P. Loh, *MRS Bulletin*, 2015, **40**, 585–591.
- 52 G. Gao, Y. Jiao, F. Ma, Y. Jiao, E. Waclawik and A. Du, 2015, <http://eprints.qut.edu.au/84406>.
- 53 Z. Zhou and J. Yuan, *Phys. Rev. A*, 2008, **77**, 063411.
- 54 M. H. Brodsky, M. Cardona and J. J. Cuomo, *Phys. Rev. B*, 1977, **16**, 3556–3571.
- 55 R. Wang, G. Zhou, Y. Liu, S. Pan, H. Zhang, D. Yu and Z. Zhang, *Phys. Rev. B*, 2000, **61**, 16827–16832.
- 56 X. Wang, S. Yang, J. Wang, M. Li, X. Jiang, G. Du, X. Liu and R. H. H. Chang, *Journal of Crystal Growth*, 2001, **226**, 123–129.
- 57 F. J. Manjón, B. Mari, J. Serrano and A. H. Romero, *J. Appl. Phys* 2005, **97**, 053516.
- 58 N. H. Nickel, F. Friedrich, J. F. Rommeluère and P. Galtier, *Appl. Phys. Lett.*, 2005, **87**, 211905.
- 59 S. -S. Lo and D. Huang, *Langmuir*, 2010, **26**, 6762–6766.

The table of contents entry: Strong anti-Stokes hyper-Raman scattering was observed in nanomaterials with large second-order susceptibilities by using femtosecond laser pulses and many Raman inactive vibration modes were clearly revealed.

Table of Contents Graphic

